Quantifying aquifer heterogeneity using superparamagnetic DNA particles

Chakraborty, Swagatam; Alqrinawi, Fuad; Foppen, Jan Willem; Schijven, Jack

DOI
10.1016/j.jconhyd.2024.104454

Publication date
2024

Document Version
Final published version

Published in
Journal of Contaminant Hydrology

Journal of Contaminant Hydrology 268 (2025) 104454

Contents lists available at ScienceDirect

Journal of Contaminant Hydrology

journal homepage: www.elsevier.com/locate/jconhyd

Quantifying aquifer heterogeneity using superparamagnetic DNA particles

Swagatam Chakraborty [a,*], Fuad Alqrinawi [b], Jan Willem Foppen [d], Jack Schijven [a,c]

[a] Environmental Hydrogeology Group, Department of Earth Sciences, Utrecht University, Princetonlaan 8a, 3584 CB Utrecht, the Netherlands
[b] Department of Water Sciences and Engineering, IHE-Delft, Institution for Water Education, Westvest 7, 2611 AX Delft, the Netherlands
[c] Department of Statistics, Informatics and Modelling, National Institute of Public Health and the Environment, P.O. Box 1, 3720 BA Bilthoven, the Netherlands
[d] Water Resources Section, Department of Civil Engineering and Geosciences, Delft University of Technology, Delft, the Netherlands

ARTICLE INFO

Keywords:
Colloids
DNA particles
Aquifer heterogeneity
Conductivity
Porosity
Sand tank

ABSTRACT

Identifying and determining hydraulic parameters of physically heterogeneous aquifers is pivotal for flow field analysis, contaminant migration and risk assessment. In this research, we applied a novel uniquely sequenced DNA tagged superparamagnetic silica microparticles (SiDNAmag) to quantify hydraulic parameters and associated uncertainties of a heterogeneous sand tank. In the sand tank with lens shaped heterogeneity, we conducted three sets of multi – point injection experiments in unconsolidated (1) homogeneous (zone 0), (2) heterogeneous with a no-conductivity-zone (zone 1), and (3) heterogeneous with a high-conductive-zone (zone 2). From the breakthrough curves (BTC), we estimated the parameters distributions of hydraulic conductivity (k), effective porosity (n_e), longitudinal dispersivity (α_L), transverse vertical (α_{TV}), and transverse horizontal dispersivities (α_{TH}) applying Monte Carlo simulation approach for BTC fitting. The estimated parameters and associated uncertainties for each of the heterogeneous sections were further statistically compared (distribution non-specific Mann Whitney *U* test) these parameter distributions with parameter distributions estimated from the conservative salt tracer. While the time of arrival and time to peak concentration of SiDNAmag and salt in effluent were comparable, peak concentration of SiDNAmag was 1–3 log reduced as compared to the salt tracer due to first order kinetic attachment. Nonetheless, the parameters and associated uncertainty distributions (5 %–95 %) of K, n_e, α_L, α_{TV}, and α_{TH}, determined from SiDNAmag BTCs were statistically equivalent to the salt tracer in all three experiment systems. Through our experimental and modelling approach, our work demonstrated that in a coarse to very coarse grain sand medium, with lens shaped heterogeneity, the uniquely sequenced SiDNAmag were a promising tool to identify heterogeneity and determine hydraulic parameters and associated uncertainty distributions.

1. Introduction

Estimation of spatial variability of aquifer hydraulic parameters is essential to accurately predict groundwater flow fields, migration of contaminant plumes, design groundwater remediation strategies, and manage groundwater resources sustainably (Cardenas and Jiang, 2010; Vincent Henri and Harter, 2019; Cardiff et al., 2013; Liu et al., 2020; Torkzaban et al., 2019; Harvey et al., 1993). Multi-point pumping tests, hydraulic head response observations, flowmeter tests, individually or in combination with geological descriptions (Cardiff et al., 2013; Maier et al., 2022; Song et al., 2023; D'Oria and Zanini, 2019; Zha et al., 2019; Mohammaddost et al., 2024), and application of tracers (Müller et al., 2010; Moeck et al., 2017; Song et al., 2023; Hartog et al., 2010; Hoffmann et al., 2019; Assari and Mohammadi, 2017) are the common approaches to assess aquifer physical heterogeneities.

In laboratory and field scales, conservative tracers (e.g. tritium, chloride, dye tracers) have been applied to determine the spatial variations in hydraulic conductivity (Salamon et al., 2007; Ronayne et al., 2010; Danquigny et al., 2004), dispersivity (Vereecken et al., 2000; Castro-Alcalá et al., 2012; Jose et al., 2004), and colloids (e.g. bacteria, virus, microspheres) have been widely used to identify the effect of physical heterogeneity on contaminant transport (Wang et al., 2013; Fontes et al., 1991; Yin et al., 2022; Sarris et al., 2018; Baumann and Werth, 2005). The effect of physical heterogeneity on the tracer transport were commonly analysed through moment analysis (Vereecken et al., 2000); deterministic or stochastic breakthrough curve fitting (Salamon et al., 2007; Ronayne et al., 2010; Dann et al., 2008; Levy and Berkowitz, 2003), tracer transport imaging (Castro-Alcalá et al., 2012; Jose et al., 2004; Baumann and Werth, 2005), or hydraulic tomography (Illman et al., 2012). The variety of investigated physical heterogeneities

* Corresponding author.

https://doi.org/10.1016/j.jconhyd.2024.104454
Received 27 May 2024; Received in revised form 29 September 2024; Accepted 31 October 2024
Available online 4 November 2024

in laboratory 3D models, in existing literatures included discrete or clustered lenses (Salamon et al., 2007; Ronayne et al., 2010; Illman et al., 2012), sand blocks (Levy and Berkowitz, 2003; Castro-Alcalá et al., 2012; Danquigny et al., 2004), and variably conductive channels (Vereecken et al., 2000; Dann et al., 2008; Derouane and Dassargues, 1998; Wang et al., 2013). Columns were typically constructed with contrasting permeability at the core, surrounded by a contrasting matrix (Morley et al., 1998; Baumann and Werth, 2005). Though laboratory sand tank models can oversimplify the complexity of real heterogeneous system, however, as compared to columns, laboratory 3D sand tank models impart more advantages and flexibilities of controlled boundary conditions with varying sink or source terms, multiple hydraulic tests, and tracer tests with horizontally and vertically distributed tracer injection and sampling locations (Mohammadi et al., 2021). Larger sand grains typically constituted the higher conductivity or velocity zones due to higher void to solid ratio (Ren and Santamarina, 2018), and lower effective porosity for the sand grain larger than ~700 - 800 μm (Urumović and Urumović Sr, 2014). Based on the scale of heterogeneity, both the solute tracers and colloid breakthrough curves reflected the effect of differential flow fields in its' asymmetry with long tailings (Bradford et al., 2004), or multi-peaked breakthrough curves (Wang et al., 2013; Yin et al., 2022). The multi – peaks were due to high velocity of solute and colloid through high conductivity zones followed by a second peak due to transport through low conductivity zones (Wang et al., 2013; Dong et al., 2019; Fontes et al., 1991; Torkzaban et al., 2019; Bhattacharjee et al., 2002). Dispersion coefficient of both the solute and colloids increased in high conductivity zones since plume expansion was directly proportional to the advection velocity (Sun et al., 2001). Colloid deposition coefficient, in most cases, were lower in high conductivity regions as compared to the low conductivity zones (Sun et al., 2001; Dong et al., 2019; Morley et al., 1998), due to enhanced hydrodynamic forces exerted on solutes or colloids by higher flow velocity (Mohammadi et al., 2019) and larger voids to migrate through (Zhang et al., 2015; Bradford et al., 2009). In columns, colloid deposition profiles explained that along with the column inlet, the interface of the high and low conductive domains (Bradford et al., 2004; Wang et al., 2013) were pivotal for colloid retention. In the systems free from colloid size dependent exclusion, colloid aggregation, and pore clogging, which often lead to velocity enhancement, reduction in hydraulic conductivity and effective porosity (Oudega et al., 2021; Mikutis et al., 2018; Won et al., 2020), hydraulic parameters (hydraulic conductivity and effective porosity) estimated from salt breakthrough curves could explain colloid transport velocity well (Bradford et al., 2004; Wang et al., 2013; Morley et al., 1998; Baumann and Werth, 2005; Maxwell et al., 2003).

Due to spatial variation of hydraulic parameters in a heterogeneous aquifer, a unique deterministic description of the system is not possible (Ptak et al., 2004; Fu and Gómez-Hernández, 2009). Neglecting the hydraulic parameter uncertainties might lead to erroneous description of the system (Rojas et al., 2008), and eventually inaccurate groundwater flow or solute transport predictions. Therefore, stochastic methods are required to acknowledge and identify the simulation, prediction and hydraulic parameter uncertainties (Ptak et al., 2004; Varouchakis and Hristopulos, 2013; Renard et al., 2013; Pool et al., 2015). Monte Carlo algorithm is one such robust stochastic tool to assess aquifer hydraulic parameter values and associated uncertainties (Fu and Gómez-Hernández, 2009; Hoffmann et al., 2019; Chakraborty et al., 2023), or spatial variations of hydraulic parameters (Herrick et al., 2002; Liang and Zhang, 2013) to predict state variables (Hoffmann et al., 2019) or assess pollution risk (Neshat et al., 2015).

Over the last fifteen years, DNA particles, encapsulated in polylactic acid, silica, or alginate (Foppen, 2023), had been used in determining subsurface flow properties, contaminant transport and characterizing aquifer hydraulic parameters (Mikutis et al., 2018; Pang et al., 2020; Zhang et al., 2021; Kong et al., 2018; Kianfar et al., 2022). Encapsulated DNA particles, unlike conventional salt tracers, could be used for concurrent injection experiments due to the uniqueness of DNA sequences without background concentration interference (Pang et al., 2020; Chakraborty et al., 2023). The additional advantages of the encapsulated DNA particles were high detection specificity in polymerase chain reaction (Dahlke et al., 2015; Foppen et al., 2011), and stability against physico – chemical parameters (pH, radiation, and enzymatic activities) because of the encapsulation (Pang et al., 2020; Mikutis et al., 2018; Sharma et al., 2012).

We previously demonstrated the suitability of SiDNAmag for hydraulic parameters estimation of a homogeneous system (Chakraborty et al., 2023). In this study, our objective was to assess the suitability of using SiDNAmag to estimate hydraulic parameter values (K, n_e, and α_L) and associated uncertainties in a homogeneous aquifer and each of the heterogeneous sections of a heterogeneous sand tank, and statistically compare the parameter value distributions with the salt tracer. To our knowledge, this is the first attempt to apply SiDNAmag to quantify the hydraulic parameter distributions (K, n_e, and α_L) of each of the heterogeneous sections of a heterogeneous aquifer using Monte Carlo simulation method. Based on the observed transport behaviour of SiDNAmag in a homogeneous sand tank, with similar sand grain size to this study (Chakraborty et al., 2023), we hypothesize that in small scale coarse grain to very coarse grain sand medium, with simple lens shaped physical heterogeneity, the hydraulic parameter distributions estimated from SiDNAmag breakthrough curves would be statistically similar to the salt tracer. Thus, SiDNAmag would be a suitable candidate to identify and determine the hydraulic parameters values and associated uncertainties of each of the heterogeneous sections in an aquifer.

2. Materials and methodology

2.1. SiDNAmag

Sharma et al. (2021), synthesized the SiDNAmag by binding negatively charged double stranded DNA (ds – DNA) onto positively charged iron oxide nanoparticles, followed by encapsulation in a silicate layer. We acquired two uniquely sequenced SiDNAmag ($SiDNAmag_1$ and $SiDNAmag_2$) stock suspensions (~10^{10} particles/ml) (NTNU, Norway) dispersed in demineralized water. The diameters of the two SiDNAmag were 184 ± 58 and 206 ± 86 nm, respectively. The zeta potentials (ζ) were – 14 and − 11 mV, when dispersed in demineralized water.

2.2. Conservative salt tracer and SiDNAmag suspension

We prepared the injection NaCl (J. T. Baker, the Netherlands) salt solution at a concentration of 1.8 g/l (pH ~7; EC ~2950 μS/cm; 0.03 M) to ensure sufficient contrast against the background tap water (EC ~480 μS/cm) in the sand tank. SiDNAmag injection suspensions were prepared as detailed in Chakraborty et al. (2023). In brief, we diluted the SiDNAmag stock suspensions with 5 ml demineralized water and treated with 1 μl commercial bleach to digest any non-encapsulated DNA present in the suspension. Then, we magnetically separated the SiDNAmags and washed twice with demineralized water to remove traces of bleach. Finally, we dispersed the magnetically separated and washed SiDNAmags in 500 ml of 5 mM phosphate buffer (~10^6 particles/ml) and used as injection suspensions. 5 mM phosphate buffer was prepared by dissolving 0.77 g/L of $Na_2HPO_4{\cdot}7H_2O$ (2.9 mM) (EMSURE®, Merck KgaA, Germany) and 0.29 g/l of $Na_2HPO_4{\cdot}7H_2O$ (2.1 mM) (J. T. Baker, Spain) in demineralized water. We used 100 mM NaOH (J. T. Baker, Poland) to adjust the pH to 7–7.1. We measured the hydrodynamic diameters (D_{hyd}) and the zeta (ζ) – potentials (at a particle concentration ~ 10^7 particles/ml) of SiDNAmags in 5 mM phosphate buffer using Smoluchowski's equation (Malvern Panalytical Zetasizer Nano-Zs ZEN 3600, the Netherlands). The D_{hyd} were measured using 173° dynamic light backscattering. To explore the interaction behaviour between the SiDNAmag and sand, we also measured the ζ – potentials of the ground sand fractions dispersed in 5 mM phosphate buffer at a *w/v* of 0.1 g/ml for both the sand fractions (500–700 μm and 1300–1600 μm) used to create the heterogeneity.

2.3. Sand tank experiments and sample analysis

We wet packed a PVC tank (1.3 m × 0.7 m × 0.4 m) with coarse grain (d = 500–700 μm; d_{50} = 630 μm) quartz sand (Sibelco, Belgium) to represent a homogeneous unconsolidated aquifer (zone 0) To create the no conductivity zone (zone 1) in the heterogeneous tank, we embedded a ~ 6 cm thick and ~ 28 cm long solid lens, shape adopted from Lu et al. (2018), at a height of ~14 - 20 cm from the bottom of the tank (Fig. 1). A wireframe of the same lens as zone 1 filled with very coarse (1300–1600 μm) sand grains, was embedded at a height of ~14 - 20 cm from the bottom of the tank to create a high conductivity zone (zone 2). In the heterogeneous systems, the zone 1 and 2 were installed in the middle of the transport length, flanked by a strip of 0.15 m of 500–700 μm sand (i.e. zone 0). We installed two fully penetrating injection wells (W_O and W_A) 0.4 m downstream of the inflow chamber. We placed a multi-level sampling well at 0.6 m downstream of the injection point on the same flowline as W_O. W_A was installed ~0.05 m transverse - perpendicularly distant from W_O (Fig. 1). We maintained a constant flow at the inflow and outflow chambers by pumping in ~796 ± 18 ml/min in the inflow chamber. The average outflow was ~781 ± 19 ml/min (measured gravimetrically) with an overall water balance percentage discrepancy of 1–4.4 %. The constant hydraulic heads were ~ 0.35 m and ~ 0.3 m the inflow and outflow chambers, respectively, with an overall hydraulic gradient of 0.037. At first, we injected 500 ml of the salt tracer into each

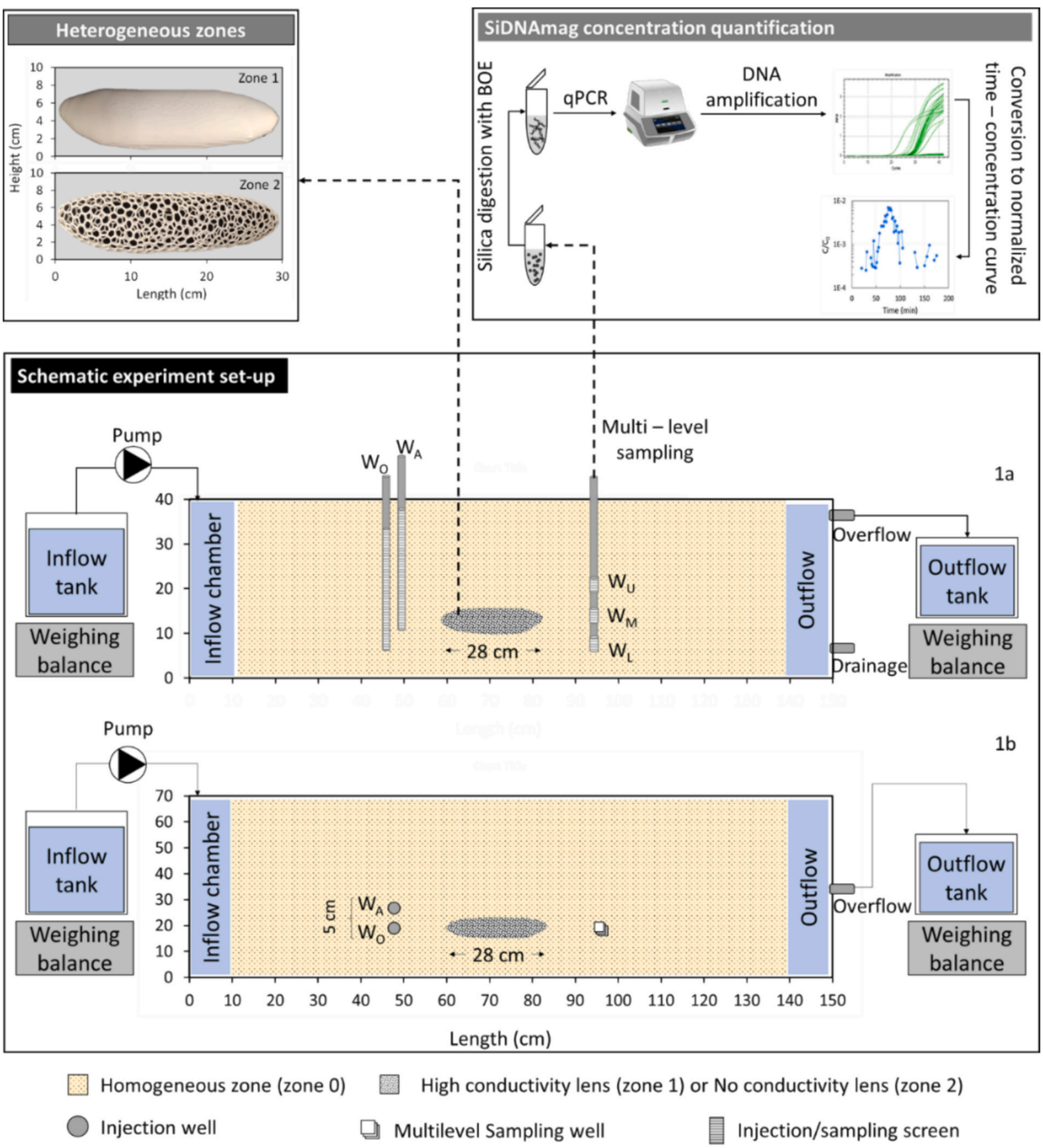

Fig. 1. Schematic vertical cross-section (1a) and top (1b) view of the experimental setup. The ~28 cm long high conductivity zone (HCZ) and no conductivity zone (NCZ) were embedded at the depth of ~14–20 cm from the bottom of the tank. The high permeability zone contained very coarse grain sand (1300–1600 μm diameter) surrounded by the coarse grain matrix (500–700 μm).

of the injection wells at a rate of ~83 ml/min for all three set ups. Since concurrent multi – point salt injection would interfere with the electric conductivity measurements injected at individual wells, we carried out the injections at W_O and W_A sequentially, after the first salt breakthrough had reduced to background concentration. After the salt injection experiments at both the injection wells were complete and the electric conductivity measurements returned to background conditions, we carried out SiDNAmag injection experiments. Due to the advantage of SiDNAmags being uniquely sequenced, we injected the SiDNAmag in both injection wells concurrently.

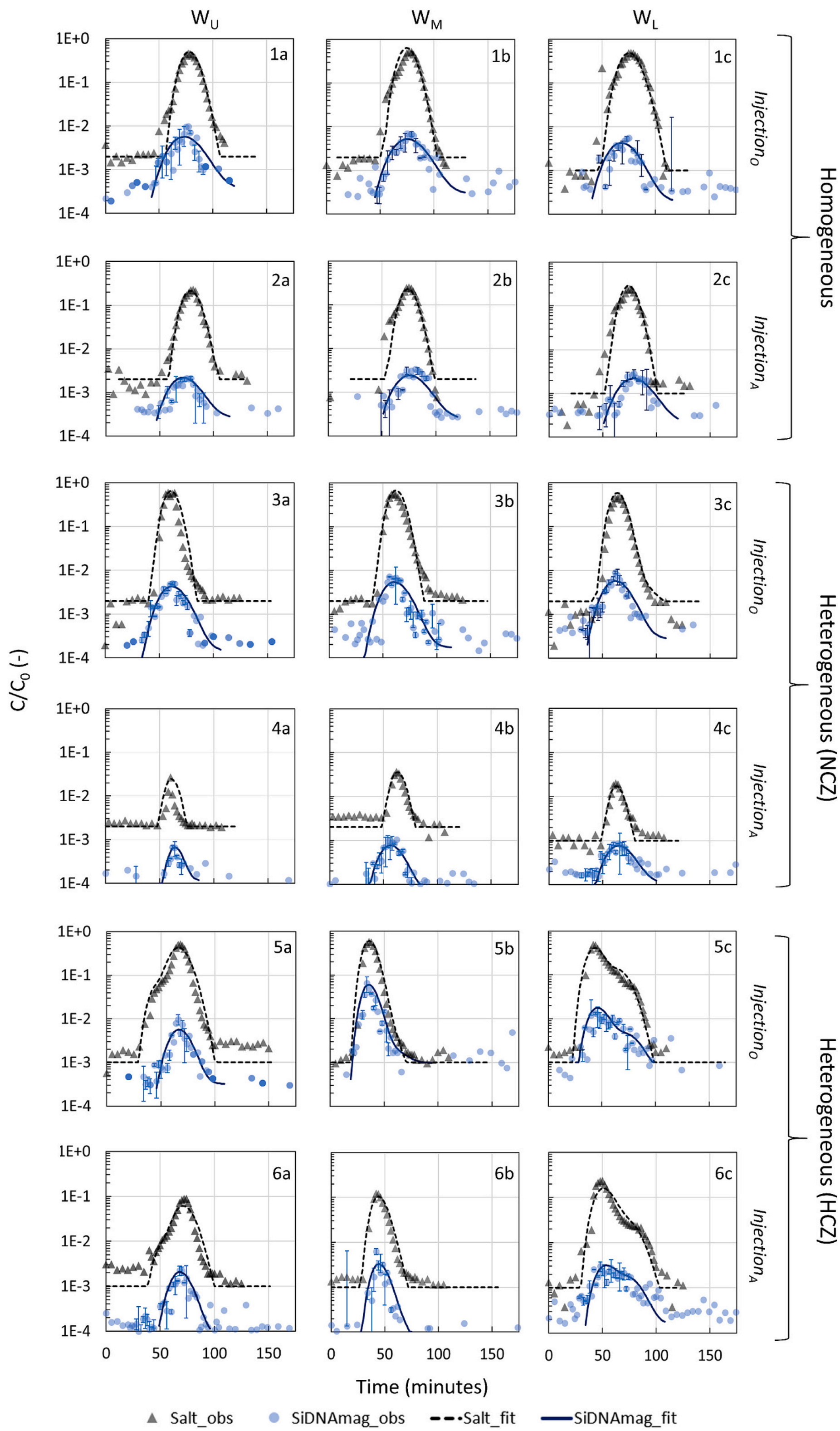

Fig. 2. Observed (_obs) and model fitted (_fit) breakthrough curves (BTCs) of the salt and the SiDNAmag transport in homogeneous (1a–2c), no conductivity zone (NCZ and zone 1) embedded (3a–4c), and high conductivity zone (HCZ and zone 2) embedded (5a–6c) sand tank. $Injection_O$ and $Injection_A$ represent the BTCs observed corresponding to the injection point On and horizontally perpendicularly Away to the flow line of sampling well, respectively.

At the multi – level sampling well, as a function of time, we determined the salt concentrations as electric conductivity (WTW-Portable conductivity meter ProfiLine Cond 3310, Germany) and the SiDNAmags as ds-DNA concentration in qPCR. The qPCR protocol for DNA concentration enumeration was as described by Chakraborty et al. (2022). Briefly, we treated 20 μL of sample with 1 μl of Buffered Oxide Etch (BOE) to dissolve the SiDNAmag. Then the sample was mixed with primers (Biolegio B.V., Nijmegen, the Netherlands) and qPCR enzyme master mix (KAPA SYBR® FAST, South Africa). Finally, the dsDNA amplification and quantification were carried out in CFX96 Touch Real Time PCR detection system (Bio-Rad laboratories, Singapore). As quality assurance, we included No Template Control (NTC) and positive controls with each set of sample analysis. In Fig. 2, the salt tracer breakthrough curve datapoints, normalized by injection concentration, were background concentration subtracted as

$$\frac{EC}{EC_0} = \frac{EC - EC_{BG}}{EC_0 - EC_{BG}} \tag{1}$$

where EC, EC_0 and EC_{BG} represented the observed, injected, and, background electric conductivity. The normalized SiDNAmag breakthrough curves present the datapoints only above NTC.

2.4. Breakthrough curve analysis

We compared the salt and the SiDNAmag breakthrough curves obtained at all three sampling locations (W_U, W_M, and W_L) from both the injection points (W_O and W_A) with regard to the shape of the breakthrough curves, time of maximum effluent concentration (t_{peak}), and maximum effluent concentrations (C_{max}/C_0). In addition, we analysed the effect of lens heterogeneities on the salt and the SiDNAmag breakthrough shapes between homogeneous, heterogeneous with NCZ and heterogeneous HCZ sand tanks.

2.5. Salt and SiDNAmag transport modelling

SiDNAmag transport through saturated porous media has been explained by classical convection – dispersion equation for solute transport integrated with first order attachment – detachment term (Chakraborty et al., 2022, 2023). We simulated the salt and the SiDNAmag transport in a 3D block – centred finite difference groundwater flow model, MODFLOW-2005 (Harbaugh et al., 2017), in conjunction with the mass transport module, MT3D (Zheng and Wang, 1999) using the partial differential equation

$$\mathrm{n_e}\frac{\partial \mathrm{C}}{\partial \mathrm{t}} + \mathrm{k_{att}n_eC} - \mathrm{k_{det}}\rho_\mathrm{b}\mathrm{S} = \frac{\partial}{\partial \mathrm{x_i}}\left(\mathrm{n_eD_{ij}}\frac{\partial \mathrm{C}}{\partial \mathrm{x_j}}\right) - \frac{\partial}{\partial \mathrm{x_i}}(\mathrm{n_ev_iC}) \tag{2}$$

Where n_e is the effective porosity of the sand [−], C is the concentration of the salt tracer or SiDNAmag in the water [kg/m^3], D_{ij} is the hydrodynamic dispersion coefficient tensor [m^2/min], k_{att} and k_{det} are the first order kinetic attachment and detachment rates of the colloids [1/min], v_i is the pore water velocity [m/min], S is the SiDNAmag concentration at the solid surface of the sand [kg/kg], ρ_b is the bulk density of the sand [kg/m^3] and t is the time since injection [min]. k_{att} and k_{det} are the attachment rate coefficient and detachment rate coefficients [1/min], respectively. The hydraulic conductivity (K) [m/min] was incorporated in the equation through v_i as $v_i = -(K/n_e) * i$, where i is the hydraulic gradient [−]. We used method of characteristics (MOC) scheme of advection to reduce numerical dispersion.

In the mass transport module MT3D, k_{att} and k_{det} were expressed in terms of as β [1/min] and k_d [m^3/kg] (Babakhani, 2019) as

$$\mathrm{k_{att}} = \frac{\beta}{n_e} \tag{3a}$$

and

$$\mathrm{k_{det}} = \frac{\beta}{\rho_b * k_d} \tag{3b}$$

where β is the mass transfer rate from water to sand [1/min] and k_d is the distribution coefficient [m^3/kg]. We considered straining to be insignificant since the SiDNAmag to Sand ratios for the coarse grain and very coarse grain sand were 0.0003, and 0.000013, respectively, which were well below the threshold of 0.004 (Johnson et al., 2010) or 0.003 (Bradford and Bettahar, 2006). The salt and SiDNAmag concentration in the injection water were too low to alter the viscosity and density of the injection water, therefore, we constant density transport in the modelling exercise.

2.6. Model description

We spatially discretised a 1.3 m × 0.7 m × 0.36 m model grid (resolution of 1 cm × 1 cm) into 12 layers with the first layer as unconfined and other layers as unconfined/confined. The thickness of each of the 12 layers was set to 2–3 cm in order to represent the height of the sampling screens used in the experiments. Layer 8 was set to ~1 cm to accommodate the lens height accurately. To simulate the homogeneous sand tank, the whole flow model was discretized as zone 0, which was also used as the background sand for heterogeneous sand tanks. To simulate the no conductivity (zone 1) and high conductivity (zone 2) lenses (we discretized the lenses into 1 cm × 1 cm grids and embedded within zone 0, spanning over three layers corresponding to the height of the lens (~6 cm). We temporally discretized the total mass transport simulation time into three stress periods for hydraulic head stabilization (50 min), injection (6 min), and sampling period (200 min). Since the injection points were fully penetrating, we determined the injection flow rates of each layer proportional to the thickness of the model layers such that the sum of the injection rates at each layer (Q_L) equalled to the total injection rate (Q_{Tot}) (Konikow et al., 2009), according to

$$Q_{Tot} = \sum_{L=1}^{12} Q_L \tag{4}$$

The sampling screens were specified at layer 5, 7, and 9. However, we did not specify any pumping rate for the sampling points since the sampling was done intermittently without constant pumping.

2.7. Parameter estimation (Monte Carlo simulation)

We simulated the groundwater, salt, and SiDNAmag transport in MODFLOW-2005 and MT3D using a python package, Flopy (Bakker et al., 2016). We determined the K, n_e, α_L, α_{TH}/α_L, and α_{TV}/α_L parameter distributions through Monte – Carlo simulation approach (Fig. 3). Thereto, the convection – dispersion equation (Eq. (2)) was solved for 5000 parameter sets random – uniformly drawn from predefined input ranges. The input ranges were defined for zone 0, and 2 individually instead of considering a resultant homogeneous system. All parameters for no conductivity zone (zone 1) were considered to be zero. To determine the input range of K, at first, we approximated the K for all three systems (homogeneous and heterogeneous systems with zone 1 and 2) by dividing the Darcy flux by hydraulic gradients measured at 6 different observation wells in the tank. Possibly due to the small scale of the experiments and heterogeneity, we did not observe any measurable effect of heterogeneity on the hydraulic heads. Therefore, for the high conductive zone, we approximated the K (~0.13 m/min) using Kozeny – Carman equation from the grain size distribution considering a d_{10} of 1.3 mm. The gravimetric approximation of n_e, for the coarse grain (zone 0) and the very coarse grain (zone 2) sand were 0.37 and 0.25 [−], respectively. Finally, we considered ±25–30 % of averaged K and n_e as the input ranges for Monte Carlo simulation. For no conductive zone, we set all the parameters as 'no flow'. The input range of α_L was 10^{-6}–10^{-1} [m] for both the HCZ and the matrix. The input of both α_{TH}/α_L, and α_{TV}/

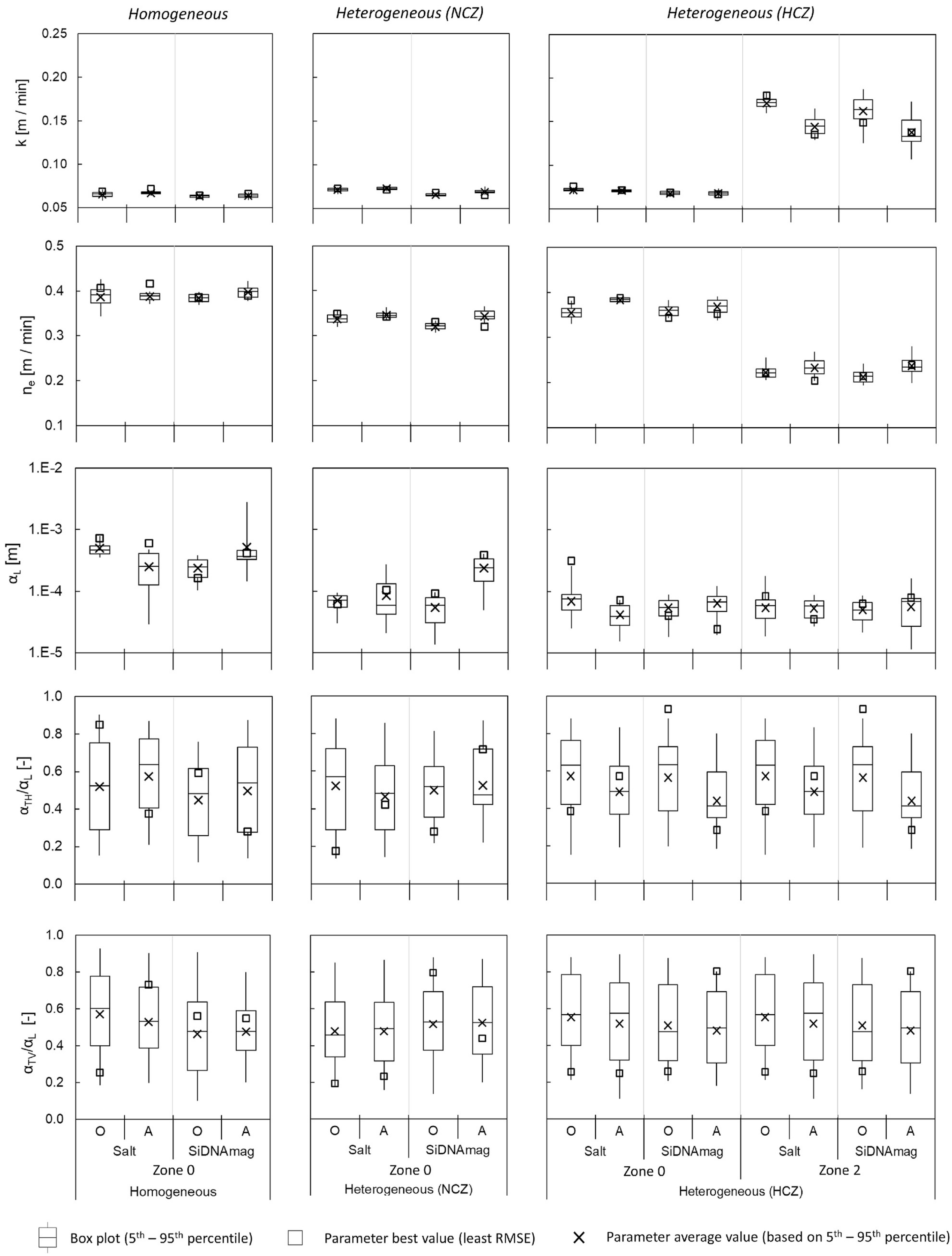

Fig. 3. Hydraulic parameter (K, n_e, α_L, α_{TH}/α_L, and α_{TV}/α_L) ranges estimated from the observed salt and SiDNAmag breakthrough curves through Monte Carlo simulation approach. 'O' and 'A' indicate the parameter distributions estimated from the injection on the sampling flowline and injection on horizontally perpendicularly away from the sampling flowline experiments. Zone 0 and Zone 2 represent the background sand (500–700 μm) and high conductive lens (1300–1600 μm).

α_L were set to a wide range of 0.01–1 [−]. The input ranges have been summarized in Table 1. Since the number of datapoints, specifically for K, were limited and defining its' distribution was not possible, we decided that the parameter sets, to be drawn for Monte Carlo simulation, to be uniformly distributed. In the post – processing, we selected the best 1 % parameter sets as the parameter distributions based on minimized Root Mean Squared Error (RMSE), both for individual sampling levels as well as for combined for all three sampling levels. RMSE was a preferred objective function over R^2 since a higher R^2 could be achieved even when the breakthrough magnitudes were not well matched (Ward et al., 2017). We evaluated the normality of the parameter distributions using Kolmogorov – Smirnov test. Since not all the distributions were normal, we applied distribution non – specific Mann Whitney *U* test ($\alpha = 0.05$) to evaluate the statistical difference between the parameter distributions. At first, we statistically compared the parameter distributions obtained from individual sampling locations with the distributions obtained from all the sampling locations combined. This was to confirm whether the distributions estimated from all sampling locations combined were good representatives of the individual sampling locations. Further, we statistically (Mann Whitney *U* test) compared the distributions estimated from the salt and the SiDNAmag breakthrough curves.

3. Results

3.1. SiDNAmag and sand characterization

The hydrodynamic diameters (D_{hyd}) of the $SiDNAmag_1$ and $SiDNAmag_2$ dispersed in 5 mM phosphate buffer were 644 ± 101, and 660 ± 108 nm, respectively. Throughout the experiment interval of 240 min, under quiescent condition, the D_{hyd} of $SiDNAmag_1$ varied between 644 and 691 nm, and 660–698 nm for $SiDNAmag_2$. Time dependent D_{hyd} had been detailed in our previous work (Chakraborty et al., 2023). The $SiDNAmag_1$ and $SiDNAmag_2$, dispersed in 5 mM phosphate buffer were negatively charged, with ζ-potentials of −44 ± 3.8, and − 41 ± 2.9 mV, respectively. The ζ-potential of the coarse grain (500 - 700 μm; used in zone 0) and very coarse grain (1300–1600 μm; used in zone 2) sand were − 50.7 ± 11.5 and − 48.3 ± 13.3 mV, respectively.

3.2. Salt and SiDNAmag breakthrough curves

In the homogeneous sand tank, both the salt and the SiDNAmag breakthrough curves were symmetric in shape. The time of maximum effluent concentration (t_{peak}) for the salt tracer and the SiDNAmags at upper (W_U), middle (W_M), and lower (W_L), sampling levels were similar.

Table 1
Input ranges of hydraulic conductivity (K), effective porosity (n_e), longitudinal dispersivity (α_L), transverse vertical (α_{TV}/α_L), and transverse horizontal (α_{TH}/α_L) dispersivity.

	Homogeneous (zone 0)	Heterogeneous (NCZ, zone 0)	Heterogeneous (HCZ, zone 2)
k [m/min]	0.048–0.081		
k_{-het} [m/min]	–	–	0.1–0.21
n_e [−]	0.27–0.46		
$n_{e\text{-}het}$ [−]	–	–	0.17–0.33
α_L [m]	10^{-6}–10^{-1}		
$\alpha_{L\text{-}het}$ [m]	–	–	10^{-6}–10^{-1}
α_{TV}/α_L [−]	0.01–1		
$\alpha_{TV}/\alpha_{L\text{-}het}$ [−]	–	–	0.01–1
α_{TH}/α_L [−]	0.01–1		
$\alpha_{TH}/\alpha_{L\text{-}het}$ [−]	–	–	0.01–1

For the salt tracer injected on the sampling flowline (W_O), the t_{peaks} were 77 min at all three sampling levels. For the injection at W_A the t_{peaks} were 75–79 min. The t_{peaks} for the SiDNAmag injected at W_O and W_A were 75–77 min and 75–79 min, respectively, and were similar to the salt tracer (Table 2). However, maximum effluent concentration (C_{max}/C_0) of SiDNAmag BTCs were 1–2 log units lower as compared to the salt tracer, for both the injection points. The ratio of SiDNAmag and the salt recovery, calculated by integrating the area under BTC, were 0.01–0.02 [−] (Fig. S1). The C_{max}/C_0 of the BTCs observed for the injection at W_A were ~ 50 % reduced since the centre of the plume was beyond the flowline of the sampling points.

In the heterogeneous tank with no conductive lens (zone 1), the t_{peaks} of the salt BTCs observed for both the injection points were 60–66 min as compared to the 56–64 min for the SiDNAmag at all three sampling levels (Table 2). While the t_{peaks} of salt and SiDNAmag BTCs were visually similar, the C_{max}/C_0 of SiDNAmag were 2–3 log units lower than the salt tracer. The recovery ratio calculated from the area under the curve of SiDNAmag to the salt were 0.014–0.092 [−]. As compared to the homogeneous system, there was no prominent effect of the zone 1 on the breakthrough curve observed from injection at W_0. However, the maximum effluent concentration of both the salt and the SiDNAmag BTCs observed from injection at W_A were reduced by 50–90 % as compared to the homogeneous system, and was the only visible effect of the no conductivity lens. This indicated the advantage of multi – point injection scheme, especially in a heterogeneous system.

There was an obvious effect of the high conductivity lens (zone 2) on the t_{peak} and the breakthrough shape. For both the injection points W_O and W_A, the t_{peaks} of salt and the SiDNAmag BTCs in the W_M and W_L were 34–42, and 42–48 min, respectively, reflected the effect of HCZ (Table 2). At W_O, the BTC falling limb sharply declined with little or no tailing, whereas, at W_L, the salt and the SiDNAmag concentrations, at the falling limb, declined with a lower slope followed by sharper decline till the background concentration (Fig. 2). The t_{peaks} of the salt and the SiDNAmag BTCs at W_U were 66–72 min since this sampling point was above the layers comprising the zone 2. However, the salt BTC at W_U was asymmetric with only a minor influence of the zone 2 on the rising limb. The SiDNAmag BTC did not capture the effect of high conductive lens at W_U. C_{max}/C_0 of SiDNAmag were reduced by 1–2 log units as compared to salt, with recovery ratio of SiDNAmag to salt of 0.015–0.087 (Fig. S1). The tailings observed in all the SiDNAmag breakthrough curves were possibly due to the SiDNAmag detachment from the collector grains. However, we did not consider these data points for parameter estimation process since the SiDNAmag concentrations at the tails were close to the no template control (NTC) measurements. Also, the breakthrough tail datapoints were of the same order of magnitude of the scattered data points prior to the SiDNAmag breakthrough. In order to avoid any possible errors in the estimated parameter uncertainties, we considered these datapoints as sample analysis error and excluded from the curve fitting and parameter estimation process.

3.3. Parameter distributions

In this section, we present the 5th–95th percentile ranges of K, n_e, α_L, α_{TH}, and α_{TV} for zone 0, and 2 for the homogeneous and the heterogeneous sand tanks. The median values of the hydraulic parameters estimated in homogeneous and heterogeneous systems have been summarized in Table 3.

In the homogeneous tank, estimated k range for the salt tracer were 0.06–0.07 [m/min] for the injection point W_O and W_A combined. The K range estimated from SiDNAmag BTCs were 0.061–0.068 [m/min], and were statistically not significantly different to the salt tracer (Table 3). The n_e ranges estimated from the salt and the SiDNAmag were 0.34–0.41, and 0.37–0.42[−], respectively. The α_L ranges estimated from the salt and the SiDNAmag ranged 3×10^{-5}–8×10^{-4} and 1×10^{-4}–2.8×10^{-3} [m]. The overall ranges of α_{TV}/α_L, and α_{TV}/α_L of the salt and the SiDNAmag were 0.1–0.9 [−]. According to the Mann

Table 2
Salt and SiDNAmag breakthrough curve characteristics (maximum concentration and time to peak) in homogeneous, heterogeneous medium with a no permeability zone (NCZ), and heterogeneous medium with a high permeability zone (HCZ) for two injection points.

		Homogeneous				Heterogeneous (NCZ)				Heterogeneous (HCZ)			
		C_{max}/C_0 [−]		t_{peak} [min]		C_{max}/C_0 [−]		t_{peak} [min]		C_{max}/C_0 [−]		t_{peak} [min]	
		O	A	O	A	O	A	O	A	O	A	O	A
Salt	W_U	0.45	0.17	77	79	0.65	0.03	64	60	0.5	0.09	68	72
	W_M	0.52	0.25	77	75	0.57	0.04	60	62	0.57	0.12	36	42
	W_L	0.48	0.24	77	75	0.48	0.02	66	62	0.48	0.25	42	46
SiDNAmag	W_U	0.01	0.002	77	79	0.005	0.0006	62	62	0.01	0.002	66	68
	W_M	0.007	0.002	75	75	0.007	0.001	56	62	0.03	0.006	34	40
	W_L	0.005	0.002	75	79	0.009	0.0009	62	64	0.013	0.003	44	48

'O' and 'A' represent breakthrough curves observed from injection on the sampling flowline and injection on horizontally perpendicularly away from the sampling flow line, respectively.

Table 3
Hydraulic parameter ranges estimated from the salt and the SiDNAmag breakthrough curves through Monte Carlo approach in the homogeneous, heterogeneous with no conductivity zone (NCZ) and high conductivity zone (HCZ) systems.

Hydraulic parameters		Homogeneous		Heterogeneous (NCZ)		Heterogeneous (HCZ)	
		Salt	SiDNAmag	Salt	SiDNAmag	Salt	SiDNAmag
K [m/min]	O	0.066 (0.06–0.07)	0.064 (0.061–0.066)	0.071 (0.066–0.074)	0.066 (0.063–0.068)	0.072 (0.067–0.075)	0.068 (0.064–0.071)
	A	0.067 (0.064–0.07)	0.063 (0.06–0.068)	0.073 (0.069–0.075)	0.069 (0.065–0.075)	0.071 (0.069–0.074)	0.068 (0.064–0.073)
k_{het} [m/min]	O	–	–	–	–	0.17 (0.16–0.184)	0.16 (0.12–0.187)
	A	–	–	–	–	0.145 (0.13–0.17)	0.133 (0.11–0.17)
n_e [−]	O	0.39 (0.34–0.41)	0.38 (0.37–0.4)	0.34 (0.32–0.35)	0.32 (0.31–0.34)	0.35 (0.33–0.38)	0.36 (0.34–0.38)
	A	0.39 (0.34–0.4)	0.4 (0.38–0.42)	0.34 (0.33–0.36)	0.34 (0.33–0.37)	0.38 (0.38–0.39)	0.37 (0.34–0.39)
$n_{e\text{-}het}$ [−]	O	–	–	–	–	0.22 (0.21–0.26)	0.21 (0.19–0.24)
	A	–	–	–	–	0.23 (0.2–0.27)	0.23 (0.2–0.28)
α_L [m]	O	4.7×10^{-4} (3.5×10^{-4}– 8×10^{-4})	2.5×10^{-4} (1×10^{-4}–3.8×10^{-4})	7.2×10^{-5} (3×10^{-5}– 9×10^{-5})	5.9×10^{-5} (1.3×10^{-5}– 9.5×10^{-5})	7.5×10^{-5} (2.5×10^{-5}– 8.6×10^{-5})	5.5×10^{-5} (1.8×10^{-5}–8.9×10^{-5})
	A	2.5×10^{-4} (3×10^{-5}– 2.8×10^{-4})	3.6×10^{-4} (1.4×10^{-4}–2.8×10^{-3})	6×10^{-5} (2.1×10^{-5}– 2.7×10^{-4})	9.4×10^{-5} (4.9×10^{-5}– 4×10^{-4})	3.9×10^{-5} (1.1×10^{-5}– 7.2×10^{-5})	6.7×10^{-5} (1.9×10^{-5}–8.6×10^{-5})
$\alpha_{L\text{-}het}$ [m]	O	–	–	–	–	5.9×10^{-5} (1.9×10^{-5}– 3.8×10^{-4})	5×10^{-5} (2.1×10^{-5}–1.2×10^{-4})
	A	–	–	–	–	5.7×10^{-5} (2.7×10^{-5}– 2.6×10^{-4})	6.8×10^{-5} (1.1×10^{-5}–1.6×10^{-4})
α_{TH}/α_L [−]	O	0.52 (0.15–0.9)	0.48 (0.12–0.76)	0.57 (0.13–0.88)	0.52 (0.22–0.81)	0.63 (0.15–0.88)	0.63 (0.2–0.88)
	A	0.64 (0.21–0.87)	0.54 (0.14–0.88)	0.48 (0.14–0.86)	0.47 (0.22–0.87)	0.49 (0.19–0.83)	0.41 (0.19–0.8)
$\alpha_{TH}/\alpha_{L\text{-}het}$ [−]	O	–	–	–	–	0.63 (0.15–0.88)	0.63 (0.2–0.83)
	A	–	–	–	–	0.49 (0.19–0.83)	0.41 (0.19–0.8)
α_{TV}/α_L [−]	O	0.6 (0.19–0.93)	0.48 (0.1–0.9)	0.46 (0.18–0.85)	0.53 (0.14–0.88)	0.57 (0.21–0.88)	0.47 (0.2–0.88)
	A	0.53 (0.2–0.9)	0.48 (0.2–0.8)	0.49 (0.16–0.86)	0.53 (0.2–0.87)	0.58 (0.11–0.89)	0.49 (0.18–0.8)
$\alpha_{TV}/\alpha_{L\ \text{-het}}$ [−]	O	–	–	–	–	0.57 (0.21–0.88)	0.47 (0.16–0.88)
	A	–	–	–	–	0.58 (0.11–0.89)	0.49 (0.14–0.8)
β [1/min]	O	–	0.021 (0.02–0.021)	–	0.023 (0.022–0.023)	–	0.021 (0.018–0.021)
	A	–	0.017 (0.015–0.02)	–	0.025 (0.024–0.028)	–	0.018 (0.015–0.022)
β_{het} [1/min]	O	–	–	–	–	–	0.022 (0.013–0.033)
	A	–	–	–		–	0.025 (0.013–0.033)
k_{att} [1/min]	O	–	0.055 (0.052–0.057)	–	0.073 (0.07–0.077)	–	0.06 (0.049–0.071)
	A	–	0.042 (0.036–0.048)	–	0.073 (0.067–0.078)	–	0.049 (0.042–0.065)
$k_{att\text{-}het}$ [1/min]	O	–	–	–	–	–	0.11 (0.058–0.163)
	A	–	–	–	–	–	0.11 (0.056–0.153)
RMSE [−]	O	0.02–0.042	0.0007–0.00072	0.034–0.041	0.0005–0.0006	0.041–0.055	0.0033–0.0043
	A	0.014–0.018	0.00028–0.00035	0.002–0.003	0.00009–0.0001	0.004–0.006	0.00037–0.00042
$A_{SiDNAmag/Salt}$ [−]	O	0.01–0.02		0.014–0.023		0.015–0.087	
	A	0.014–0.02		0.029–0.092		0.025–0.029	

The parameter values are represented as median (5th–95th percentile range). $A_{SiDNAmag/Salt}$ is the SiDNAmag to salt ratio of area under the curve (recovery).

Whitney *U* test (α = 0.05), the parameter distributions of n_e, α_L, α_{TH}/α_L, and α_{TV}/α_L determined from the SiDNAmag BTCs were statistically not different from the salt tracer. The first order mass transfer rate (β) of SiDNAmag onto the coarse grain sand were 0.021 and 0.017 [1/min] for W_O and W_A, respectively, corresponding to the attachment rate coefficients (k_{att}s) of 0.055 and 0.042 [1/min]. The SiDNAmag to salt recovery ratio, combined for both the injection points W_O and W_A, ranged between 0.01 and 0.02 [−] (Table 3). The linear water flow velocity estimated from the K, n_e distributions and hydraulic gradient from salt tracer ranged between 0.0061 and 0.0065 [m/min], as compared to 0.058–0.062 [m/min] from SiDNAmag breakthrough curves. The average linear velocity estimated from both the salt and the SiDNAmag BTCs were statistically equivalent.

In the heterogeneous system (with embedded zone 1), we estimated the hydraulic and mass transport parameters only for the zone 0, since we considered all parameters to be zero for no conductivity zone 1. The K ranges estimated from salt BTCs for both injection points combined were 0.066–0.075 [m/min] as compared to 0.063–0.075 [m/min] estimated from SiDNAmag BTCs. The n_e range estimated from the salt tracer BTCs for both the injection points were 0.33–0.36[−]in comparison with 0.31–0.37 [−] estimated from the SiDNAmag. The α_L range of the salt tracer BTCs estimated from both the injection points were 2.1×10^{-5}– 2.7×10^{-4} [m] as compared to 1.3×10^{-5}–4×10^{-4} [m] estimated from SiDNAmag BTCs. The α_L of the SiDNAmag and salt tracer in heterogeneous (NCZ) tank were ~ 40–50 % lower than the homogeneous tank. The α_{TV}/α_L, and α_{TV}/α_L of the salt tracer ranged between 0.13 and 0.88 [−], whereas, the α_{TH}/α_L, and α_{TV}/α_L of the SiDNAmag ranged between 0.14 and 0.88 [−], and were statistically not different from the salt tracer. According to the Mann Whitney *U* test, the parameter distributions of K, n_e, α_L, α_{TV}/α_L, and α_{TV}/α_L of zone 0, determined from the SiDNAmag BTCs were statistically not significantly different from the salt tracer. The first order mass transfer rate (β) of SiDNAmag onto the coarse grain sand in matrix were 0.023 and 0.025 [1/min] for W_O and W_A, respectively, both corresponding to a k_{att} of 0.073 [1/min]. The SiDNAmag to salt recovery ratio, combined for both the injection points W_O and W_A, ranged between 0.014 and 0.092 [−] (Table 3).

In the heterogeneous tank with embedded zone 2, the K range of the zone 0 estimated from the salt BTCs for two injection points was 0.067–0.075 [m/min] The K range of the high conductivity lens (zone 2) estimated from salt tracer BTCs was 0.13–0.18 [m/min]. The K range of the zone 0 estimated from the SiDNAmag BTCs was 0.064–0.073 [m/min]. The K range of the zone 2 estimated from the SiDNAmag BTCs was 0.11–0.18 [m/min]. The n_e range of the zone 0 and 2, estimated from the salt tracer were 0.33–0.39 and 0.2 and 0.27[−], respectively. The range of n_e for zone 0 and 2, estimated from SiDNAmag were 0.34–0.39, and 0.2–0.28 [−], respectively. The median n_e of the zone 2, estimated from both the salt tracer and the SiDNAmag, were ~ 40–50 % lower than the zone 0. The α_L range of the zone 0 and 2, estimated from the salt tracer BTCs, were 1.1×10^{-5} - 8.6×10^{-5}, and 1.9×10^{-5}– 3.8×10^{-4} [m], respectively. The α_L range of the zone 0 and 2, estimated from the SiDNAmag BTCs, were 1.8×10^{-5}–8.9×10^{-5}, and 1.1×10^{-5}– 1.6×10^{-4} [m], respectively. The 5th–95th range of α_L of the zone 2 were in the same order of magnitude as the zone 0 and were statistically similar. The α_{TH}/α_L, and α_{TV}/α_L ranges of the zone 0 estimated from the salt and the SiDNAmag 0.11–0.89, and 0.18–0.88 [−], respectively. The α_{TH}/α_L, and α_{TV}/α_L ranges of the zone 2 estimated from the salt and the SiDNAmag 0.11–0.89, and 0.14–0.88 [−], respectively. According to the Mann Whitney *U* test, the k, n_e, α_L, α_{TH}/α_L, and α_{TV}/α_L ranges of the salt and the SiDNAmag, both in the zone 0 and 2, were statistically not significantly different. The first order mass transfer rate (β) of SiDNAmag onto the coarse grain sand in zone 0 were 0.021 and 0.018 [1/min] for W_O and W_A, respectively, corresponding to k_{att}s of 0.06 and 0.049 [1/min]. In the very coarse grain sand in zone 2, β were 0.022 and 0.025 [1/min], both corresponding to a k_{att} of 0.11 [1/min]. The recovery ratio of SiDNAmag to salt tracer, combined for both the injection points W_O and W_A, ranged between 0.015 and 0.087 [−] (Table 3). The RMSE ranges corresponding to each set up and injection points are summarized in Table 3.

Based on the minimized objective function (RMSE) and best 1 % of the Monte – Carlo simulation parameter sets, the parameter distributions estimated from BTCs observed at individual sampling depth (W_U, W_M, and W_L) were statistically similar to the parameter distributions estimated from all sampling depths combined. Therefore, here we presented only the parameter distributions estimated from the sampling points combined. The best parameter set for BTCs observed at individual sampling point have been summarized in the supplementary information (Table S1).

4. Discussion

The convective – dispersive flow and solute transport module could satisfactorily explain the salt BTCs, and the SiDNAmag BTCs with first order kinetic attachment rate coefficient incorporated. The similar time to peak (t_{peak}s), and statistically similar uncertainties of K, n_e, α_L, α_{TH}, and α_{TV} values estimated from the salt tracer and SiDNAmag in zone 0 and zone 2 of the homogeneous and heterogeneous sand tanks indicated that in our experimental condition, SiDNAmag and salt tracer exhibited similar convective – dispersive transport behaviour, and complied with our hypothesis.

The similar t_{peak}s of the salt tracer and the SiDNAmag BTCs in both the homogeneous and heterogeneous sand tanks (with zone 1 and 2) at all sampling points indicated that the SiDNAmags migrated with the velocity almost identical to the salt tracer. With the sand grain size to colloid ratio similar to this study (3000 and 7000 [−] for coarse grain and very coarse grain sand, respectively), similar mean transport velocity of conservative tracer and colloids were reported by Chakraborty et al. (2023); Chrysikopoulos and Katzourakis (2015); Solovitch et al. (2010); and Bradford and Leij (2018). Therefore, the often observed phenomenon of size exclusion and velocity enhancement (Mikutis et al., 2018; Grolimund et al., 1998) did not occur visibly in both the coarse grain (zone 0) and very coarse grain (zone 2) sand, possibly due to the pore throat to SiDNAmag ratio being atleast two orders of magnitude higher than the threshold value of ~1.5 (Sirivithayapakorn and Keller, 2003).

4.1. Breakthrough behaviour

In the homogeneous tank, both the salt and the SiDNAmag BTCs were almost symmetric with little or no tailing, suggesting uniform homogeneous flow of the salt and SiDNAmag (Ghosh et al., 2022; Chakraborty et al., 2022). Though we measured few samples with near – NTC SiDNAmag concentrations in the SiDNAmag BTC tails, however, we considered these datapoints as sample analysis error since we observed SiDNAmag concentrations of similar order of magnitude prior to the breakthrough as well. The effect of heterogeneity (with zone 1) was not apparent on the salt and SiDNAmag BTCs observed for injection at W_O, which was due to the re-mergence of salt and SiDNAmag plume past the no conductivity zone and migrating similar to the homogeneous zone (Fig. S5b). Therefore, a reduction in the maximum effluent concentration by 50–90 % observed in the BTCs for injection at W_A demonstrated the significance of conducting multi – point tracing in identifying a no conductivity zone. Breakthrough tailing of conservative tracers and colloids were commonly observed due to slow release of the tracers or back diffusion from low permeability zones (Chapman et al., 2012; Tatti et al., 2016; Qin et al., 2020). Breakthrough tailings were not observed in our experiment since the lens used in our work was 'no' flow lens, as also observed by Leij and Bradford (2013), when low permeability lens had little or no flow velocity. The effect of zone 2 on the BTCs, observed at W_U and W_L, were obvious in the breakthrough shape. In W_L, the first peaks were due to the influence of higher conductivity and flow velocity in the high conductivity zone 2 followed by the second peaks due to the lower conductivity matrix. This was similar to the multi – peaked BTCs observed by Wang et al. (2013); Yin et al. (2022); and, Dong et al. (2019) due to faster tracer transport through high conductivity zones or lenses. In W_M, like heterogeneity with zone 1, there was no prominent effect of the high conductivity zone 2 on the breakthrough shape other than overall faster transport (faster t_{peak}), due to the plumes transported similar to the homogeneous system once past the HCZ (Fig. S5c).

4.2. Estimated parameter value uncertainties

The initial input ranges and the estimated hydraulic conductivity of the coarse grain (zone 0) and very coarse grain (zone 2) sand were well within the realistic ranges of 0.00006–0.6 [m/min] for clean sand and 0.006–60 [m/min] for gravelly sand (Freeze and Cherry, 1979; Sosa et al., 2022). While a number of studies have reported enhancement or reduction in hydraulic conductivity due to adaptation of preferential flow paths or colloid attachment onto the sand grains or pore clogging (Oudega et al., 2021; Keller et al., 2004; Dikinya et al., 2008; Won and Burns, 2017), Wang et al. (2013), demonstrated that colloids migrated more or less like conservative tracer when the colloid size is sufficiently small. Though Hong et al. (2009), and Roychowdhury et al. (2014), demonstrated that even for smaller colloids aggregation played a pivotal role in straining or pore clogging, we did not observe significant change in the D_{HYD} throughout the experiment duration. Chakraborty et al.

(2023), in a homogeneous sand tank, demonstrated that hydraulic conductivity estimated from NaCl tracer was statistically equivalent to SiDNAmag. Both in the homogeneous and heterogeneous systems, studies with ~1 order of magnitude lesser collector to colloid ratio as compared to the present work, could explain the colloid transport using the hydraulic conductivity estimated from conservative tracer (Bradford et al., 2004; Baumann and Werth, 2005; Lyon-Marion et al., 2017; Leij and Bradford, 2013). Since the viscosity and density of the injection suspension were not significantly different than the background water in the tank, a reduction in the estimation of hydraulic conductivity by resisting the plume movement (Li et al., 2016; Mondal et al., 2018) was not expected.

In homogeneous, heterogeneous (with zone 1), and heterogeneous (with zone 2) sand tanks, the effective porosity and associated uncertainty ranges estimated from SiDNAmag BTCs were statistically similar to the salt tracer in both the coarse grain and very coarse grain sand. This agreed with the findings that, when the colloid diameter was sufficiently small to migrate similar to a conservative tracer (Wang et al., 2013), effective porosity estimated from conservative tracers could explain colloid BTCs satisfactorily (Tian et al., 2010; Tosco et al., 2009). Though colloid attachment had been reported to reduce effective porosity (Li et al., 2016; Chrysikopoulos and Katzourakis, 2015), and SiDNAmag attachment occurred in our experiments, however, was probably not enough to influence the pore structure and the effective porosity (Liu et al., 2016). The estimated effective porosity of the very coarse grain sand (zone 2) (~0.22 [−]) was less than the coarse grain (zone 0) effective porosity (~0.37 [−]), which agreed with the observation that effective porosity reduced for sand grain diameter > 700–800 μm as per Castany, 1967 (Huysmans and Dassargues, 2005).

Both in the coarse grain (zone 0) and very coarse grain (zone 2) sand, in the homogeneous and heterogeneous sand tanks, the longitudinal dispersivities and associated uncertainties of SiDNAmag were statistically not significantly different from the conservative salt tracer. Similar observations were also reported by Tian et al. (2010),Keller et al. (2004), and Chakraborty et al. (2023). This was possibly due to the small size of SiDNAmag, since smaller particles took more detours as compared to larger colloids (Auset and Keller, 2004; Keller et al., 2004; Sirivithayapakorn and Keller, 2003; Chrysikopoulos and Katzourakis, 2015), and migrated similar to a conservative tracer (Syngouna and Chrysikopoulos, 2011). The longitudinal dispersivity had been reported to increase in the high permeable region since dispersivity proportionally increases with advection velocity (Sun et al., 2001). Though we estimated the 95th percentile of the longitudinal dispersivity range of the salt tracer and SiDNAmag to be ~0.5 order of magnitude higher in high conductive very coarse grain (zone 2) sand as compared to zone 0, the overall value uncertainties were not statically significantly different. Therefore, our experimental and analysis method were inefficient to distinguish the longitudinal dispersivity between the lower and higher permeability regions. The median α_{TV}/α_L, and α_{TH}/α_L values of both the salt tracer and SiDNAmag, however, were higher than the usually accepted value of 0.1 (Bijeljic and Blunt, 2007). This was possibly due to low peclet number (0.5–1) and flow velocity conditions where the ratio of transverse and longitudinal dispersion coefficients could reach as high as 1 (Bijeljic and Blunt, 2007), pertaining to colloids following more tortuous flow path (He et al., 2014). However, to understand the similarity of SiDNAmag transverse dispersion with the salt tracer, a pore scale observation would be required (Baumann et al., 2010).

4.3. SiDNAmag attachment

First order kinetic attachment of SiDNAmag onto the coarse grain (zone 0) and very coarse grain sand (zone 2) resulted in 1–2 orders of magnitude reduction in SiDNAmag recovery as compared to the salt tracer, which was a limitation to overcome for subsurface application of SiDNAmag (Pang et al., 2020). In the heterogenous tank (zone 2), k_{att} in the very coarse grain sand was ~1.5–2.6 times higher as compared to the zone 0 with lower hydraulic conductivity. Considering our experimental conditions (e.g. grain size, Darcy flux) this is in accordance with the relation that particle deposition was directly proportional to the pore water velocity, inversely proportional to the effective porosity (Tufenkji and Elimelech, 2004), and directly proportional to $K^{1/3}$ (Sun et al., 2001). Though, many studies observed lesser colloid k_{att} in high conductivity zones with higher flow velocity (Dong et al., 2019; Qin et al., 2020; Wang et al., 2013; Phenrat et al., 2010; Torkzaban et al., 2019), due to enhanced hydrodynamic forces increasing pore voids for increased colloid migration (Zhang et al., 2015; Bradford et al., 2009) or by creating larger shadow zones (Ko and Elimelech, 2000). Probably our experimental condition was below a critical velocity (Ahfir et al., 2009) beyond which k_{att} would decrease at higher flow velocity.

4.4. Sensitivity to transport length and velocity

Since the BTC shapes were a prominent indicator of the high conductive channel in the heterogeneous tank with zone 2, as also observed by Wang et al. (2013); and Yin et al. (2022), we evaluated the effect of different hypothetical length of zone 0 (L_M) to length of zone 2 (L_{HCZ}) ratio (0.33–2.33 [−]) on the BTC shape indicator. We used the median k, n_e, α_L, α_{TH}/α_L, and α_{TV}/α_L for salt and SiDNAmag along with the median k_{att} for SiDNAmag. In these hypothetical L_M/L_{HCZ} ratio, the L_{HCZ} was kept constant flanked by increasing L_M. The simulated breakthrough curves (Fig. S3) indicated that increase in L_M/L_{HCZ} results in diminished multi – peak behaviour of the BTCs, resembling tracer breakthrough of a homogeneous system for both the NaCl and SiDNAmag BTCs. Therefore, in order to identify the heterogeneity and further estimate hydraulic parameters of each section with different hydraulic properties using the current method, it is important to conduct length-wise multi – point injection and sampling experiments.

Since the salt and colloid transport were velocity dependent (Dong et al., 2019; Qin et al., 2020), in addition to the transport length, we also evaluated the breakthrough behaviour as a function of different hypothetical velocity scenarios (a ratio of experimental and hypothetical velocity ranging between 0.16 and 1.32) considering the estimated median k, n_e, α_L, α_{TH}/α_L, and α_{TV}/α_L values. Though Darcy velocity can influence the large colloid dispersivities (Sun et al., 2001), we assumed our colloid size was small enough not to influence the dispersivity significantly. For SiDNAmag transport, we calculated the k_{att} at different velocity using (Tufenkji and Elimelech, 2004) -

$$k_{att} = 1.5\,\frac{(1-n_e)}{d_c n_e}\,v\alpha\eta_0 \tag{5}$$

where v was the Darcy velocity [m/min], α was the attachment efficiency [−], and η_0 was the single collector contact efficiency [−]. We considered a constant α for all velocities since theoretically α is independent of linear velocity (Tufenkji and Elimelech, 2004), and same for similar sand and colloid material (Bradford et al., 2004). The k_{att} was only an approximation since the equation is applicable for 1D system. The simulated breakthrough curves show (Fig. S4) that reduction in velocity results in visibly smoother curves with reduced effect of the high conductivity zone 2 on the breakthrough shape. Therefore, a SiDNAmag BTC resembling a homogeneous transport path does not guarantee the homogeneity of the system and it is important to conduct multi – point injection and sampling experiments at different velocities to identify the heterogeneous lens and estimate parameter ranges for each section with different hydraulic properties.

In addition, our experimental approach and results indicated that in a sand tank, packed with coarse to very coarse grain sand and with lens shape heterogeneity, SiDNAmags were suitable for determining the hydraulic parameters and associated uncertainties which were not statistically significantly different than the conventional salt tracer. However, in order to expand the suitability of SiDNAmag use, further experiments should be conducted considering different grain size, heterogeneity shape and complexity.

5. Conclusion

1. The hydraulic parameters (K, n_e, α_L, α_{TH}/α_L, and α_{TV}/α_L) and associated uncertainties estimated from SiDNAmag BTCs using Monte – Carlo simulations approach in homogeneous (zone 0), heterogeneous (with zone 1), and heterogeneous (with zone 2) sand tanks were statistically not significantly different than the salt tracer.
2. Though the α_L, α_{TH}/α_L, and α_{TV}/α_L value uncertainty ranges estimated form the salt tracer and the SiDNAmag in the heterogeneous sand tank for both the lower conductivity zone or matrix (zone 0) and higher conductivity lens (zone 2) were statistically not different, we did not observe a clear distinction of longitudinal dispersivity values between the zone 0 and zone 2, in the heterogeneous sand tank
3. In the heterogeneous tank, the effect of high conductivity lens (zone 2) was observed as a faster peak concentration for both the salt and the SiDNAmag followed by a slower peak due to the lower conductivity zone 0
4. In the heterogeneous sand tank with no conductivity zone (zone 1), the effect of zone 1 was not evident on the breakthrough time and shape observed for the injection on the flowline of sampling well. However, for the injection point horizontally perpendicularly away from the flowline, the maximum salt and SiDNAmag concentrations were ∼ 1 log unit lower as compared to the homogeneous sand tank. This indicated the relevance of multi – point injection approach for identifying aquifer heterogeneity and in turn, the advantage of applying uniquely sequenced SiDNAmag.
5. SiDNAmag attachment onto the collector grains resulted in lesser mass recovery as compared to the conservative tracer. This is a potential limitation of SiDNAmag application to determine the hydraulic parameters and associated uncertainties for longer transport distances.
6. Overall, under current experiment conditions, SiDNAmag was a suitable candidate for identifying and determining hydraulic conductivity and effective porosity values and associated uncertainty ranges in homogeneous and each heterogeneous section of the heterogeneous sand tank

CRediT authorship contribution statement

Swagatam Chakraborty: Writing – original draft, Methodology, Investigation, Conceptualization. **Fuad Alqrinawi:** Investigation. **Jan Willem Foppen:** Writing – review & editing, Supervision, Resources, Methodology, Investigation, Conceptualization. **Jack Schijven:** Writing – review & editing, Supervision, Methodology, Investigation, Conceptualization.

Declaration of competing interest

The authors declare that they have no known competing financial interests or personal relationships that could have appeared to influence the work reported in this paper.

Data availability

Data will be made available on request.

Acknowledgement

This research had been funded by the Dutch Research Council (NWO), TTW grant 14514. We would like to thank Dr. Sulalit Bandyopadhyay, Department of Chemical Engineering, Faculty of Natural Sciences, NTNU, Norway for the kind contribution with SiDNAmag particles. We would like extend our gratitude to Dr. Thom Bogaard, Department of Civil Engineering and Geosciences, TU-Delft, the Netherlands, for his contribution and support with experimental setup preparation and modelling. We would like to thank Dr. Ahmed Mahmoud (PostDoc); Ms. Yuchen Tang (PhD student); Hortus Botanicus, TU-Delft, the Netherlands; and IHE-Delft, the Netherlands for laboratory work support.

Appendix A. Supplementary data

Supplementary data to this article can be found online at https://doi.org/10.1016/j.jconhyd.2024.104454.

References

Ahfir, N.D., Benamar, A., Alem, A., Wang, H., 2009. Influence of internal structure and medium length on transport and deposition of suspended particles: a laboratory study. Transp. Porous Media 76, 289–307. https://doi.org/10.1007/s11242-008-9247-3.

Assari, A., Mohammadi, Z., 2017. Assessing flow paths in a karst aquifer based on multiple dye tracing tests using stochastic simulation and the MODFLOW-CFP code. Hydrogeol. J. 25 (6), 1679.

Auset, M., Keller, A.A., 2004. Pore-scale processes that control dispersion of colloids in saturated porous media. Water Resour. Res. 40 (3). https://doi.org/10.1029/2003WR002800.

Babakhani, P., 2019. The impact of nanoparticle aggregation on their size exclusion during transport in porous media: one-and three-dimensional modelling investigations. Sci. Rep. 9 (1), 14071. https://doi.org/10.1038/s41598-019-50493-6.

Bakker, M., Post, V., Langevin, C.D., Hughes, J.D., White, J.T., Starn, J.J., Fienen, M.N., 2016. Scripting MODFLOW model development using Python and FloPy. Groundwater 54 (5), 733–739. https://doi.org/10.1111/gwat.12413.

Baumann, T., Werth, C.J., 2005. Visualization of colloid transport through heterogeneous porous media using magnetic resonance imaging. Colloids Surf. A Physicochem. Eng. Asp. 265 (1–3), 2–10. https://doi.org/10.1016/j.colsurfa.2004.11.052.

Baumann, T., Toops, L., Niessner, R., 2010. Colloid dispersion on the pore scale. Water Res. 44 (4), 1246–1254. https://doi.org/10.1016/j.watres.2009.11.035.

Bhattacharjee, S., Ryan, J.N., Elimelech, M., 2002. Virus transport in physically and geochemically heterogeneous subsurface porous media. J. Contam. Hydrol. 57 (3–4), 161–187. https://doi.org/10.1016/S0169-7722(02)00007-4.

Bijeljic, B., Blunt, M.J., 2007. Pore-scale modeling of transverse dispersion in porous media. Water Resour. Res. 43 (12). https://doi.org/10.1029/2006WR005700.

Bradford, S.A., Bettahar, M., 2006. Concentration dependent transport of colloids in saturated porous media. J. Contam. Hydrol. 82 (1–2), 99–117. https://doi.org/10.1016/j.jconhyd.2005.09.006.

Bradford, S.A., Bettahar, M., Simunek, J., Van Genuchten, M.T., 2004. Straining and attachment of colloids in physically heterogeneous porous media. Vadose Zone J. 3 (2), 384–394. https://doi.org/10.2113/3.2.384.

Bradford, S.A., Kim, H.N., Haznedaroglu, B.Z., Torkzaban, S., Walker, S.L., 2009. Coupled factors influencing concentration-dependent colloid transport and retention in saturated porous media. Environ. Sci. Technol. 43 (18), 6996–7002. https://doi.org/10.1021/es900840d.

Bradford, S.A., Leij, F.J., 2018. Modeling the transport and retention of polydispersed colloidal suspensions in porous media. Chemical Engineering Science 192, 972–980.

Cardenas, M.B., Jiang, X.W., 2010. Groundwater flow, transport, and residence times through topography-driven basins with exponentially decreasing permeability and porosity. Water Resour. Res. 46 (11). https://doi.org/10.1002/wrcr.20064.

Cardiff, M., Bakhos, T., Kitanidis, P.K., Barrash, W., 2013. Aquifer heterogeneity characterization with oscillatory pumping: sensitivity analysis and imaging potential. Water Resour. Res. 49 (9), 5395–5410. https://doi.org/10.1002/wrcr.20356.

Castro-Alcalá, E., Fernàndez-Garcia, D., Carrera, J., Bolster, D., 2012. Visualization of mixing processes in a heterogeneous sand box aquifer. Environ. Sci. Technol. 46 (6), 3228–3235. https://doi.org/10.1021/es201779p.

Chakraborty, S., Foppen, J.W., Schijven, J.F., 2022. Effect of concentration of silica encapsulated ds-DNA colloidal microparticles on their transport through saturated porous media. Colloids Surf. A Physicochem. Eng. Asp. 651, 129625. https://doi.org/10.1016/j.colsurfa.2022.129625.

Chakraborty, S., Elhaj, R., Foppen, J.W., Schijven, J., 2023. Effect of injection water ionic strength on estimating hydraulic parameters in a 3D sand tank using silica encapsulated magnetic DNA particles. Adv. Water Resour. 104507. https://doi.org/10.1016/j.advwatres.2023.104507.

Chapman, S.W., Parker, B.L., Sale, T.C., Doner, L.A., 2012. Testing high resolution numerical models for analysis of contaminant storage and release from low permeability zones. J. Contam. Hydrol. 136, 106–116. https://doi.org/10.1016/j.jconhyd.2012.04.006.

Chrysikopoulos, C.V., Katzourakis, V.E., 2015. Colloid particle size-dependent dispersivity. Water Resour. Res. 51 (6), 4668–4683. https://doi.org/10.1002/2014WR016094.

Dahlke, H.E., Williamson, A.G., Georgakakos, C., Leung, S., Sharma, A.N., Lyon, S.W., Walter, M.T., 2015. Using concurrent DNA tracer injections to infer glacial flow pathways. Hydrol. Process. 29 (25), 5257–5274. https://doi.org/10.1002/hyp.10679.

Dann, R.L., Close, M.E., Pang, L., Flintoft, M.J., Hector, R.P., 2008. Complementary use of tracer and pumping tests to characterize a heterogeneous channelized aquifer system in New Zealand. Hydrogeol. J. 16, 1177–1191. https://doi.org/10.1007/s10040-008-0291-4.

Danquigny, C., Ackerer, P., Carlier, J.P., 2004. Laboratory tracer tests on three-dimensional reconstructed heterogeneous porous media. J. Hydrol. 294 (1–3), 196–212. https://doi.org/10.1016/j.jhydrol.2004.02.008.

Derouane, J., Dassargues, A., 1998. Delineation of groundwater protection zones based on tracer tests and transport modeling in alluvial sediments. Environ. Geol. 36, 27–36. https://doi.org/10.1007/s002540050317.

Dikinya, O., Hinz, C., Aylmore, G., 2008. Decrease in hydraulic conductivity and particle release associated with self-filtration in saturated soil columns. Geoderma 146 (1–2), 192–200. https://doi.org/10.1016/j.geoderma.2008.05.014.

Dong, S., Gao, B., Sun, Y., Guo, H., Wu, J., Cao, S., Wu, J., 2019. Visualization of graphene oxide transport in two-dimensional homogeneous and heterogeneous porous media. J. Hazard. Mater. 369, 334–341. https://doi.org/10.1016/j.jhazmat.2019.02.042.

D'Oria, M., Zanini, A., 2019. Characterization of hydraulic heterogeneity of alluvial aquifer using natural stimuli: a field experience of northern Italy. Water 11 (1), 176. https://doi.org/10.3390/w11010176.

Fontes, D.E., Mills, A.L., Hornberger, G.M., Herman, J., 1991. Physical and chemical factors influencing transport of microorganisms through porous media. Appl. Environ. Microbiol. 57 (9), 2473–2481. https://doi.org/10.1128/aem.57.9.2473-2481.1991.

Foppen, J.W., 2023. Artificial DNA in hydrology. Wiley Interdiscip. Rev. Water e1681. https://doi.org/10.1002/wat2.1681.

Foppen, J.W., Orup, C., Adell, R., Poulalion, V., Uhlenbrook, S., 2011. Using multiple artificial DNA tracers in hydrology. Hydrol. Process. 25 (19), 3101–3106. https://doi.org/10.1002/hyp.8159.

Freeze, R.A., Cherry, J.A., 1979. Groundwater. New Jersey: Prentice-Hall geochemical parameter distribution in a ground water system contaminated with petroleum hydrocarbons. J. Environ. Qual. 30, 1548–1563.

Fu, J., Gómez-Hernández, J.J., 2009. Uncertainty assessment and data worth in groundwater flow and mass transport modeling using a blocking Markov chain Monte Carlo method. J. Hydrol. 364 (3–4), 328–341. https://doi.org/10.1016/j.jhydrol.2008.11.014.

Ghosh, D., Das, S., Gahlot, V.K., Pulimi, M., Anand, S., Chandrasekaran, N., Mukherjee, A., 2022. Nano-SiO2 transport and retention in saturated porous medium: influence of pH, ionic strength, and natural organics. J. Contam. Hydrol. 248, 104029. https://doi.org/10.1016/j.jconhyd.2022.104029.

Grolimund, D., Elimelech, M., Borkovec, M., Barmettler, K., Kretzschmar, R., Sticher, H., 1998. Transport of in situ mobilized colloidal particles in packed soil columns. Environ. Sci. Technol. 32 (22), 3562–3569. https://doi.org/10.1021/es980356z.

Harbaugh, A.W., Langevin, C.D., Hughes, J.D., Niswonger, R.N., Konikow, L.F., 2017. MODFLOW-2005 version 1.12. 00, the US geological survey modular groundwater model. US Geolo. Surv. Softw. Release 3.

Hartog, N., Cho, J., Parker, B.L., Annable, M.D., 2010. Characterization of a heterogeneous DNAPL source zone in the Borden aquifer using partitioning and interfacial tracers: residual morphologies and background sorption. J. Contam. Hydrol. 115 (1–4), 79–89. https://doi.org/10.1016/j.jconhyd.2010.04.004.

Harvey, R.W., Kinner, N.E., MacDonald, D., Metge, D.W., Bunn, A., 1993. Role of physical heterogeneity in the interpretation of small-scale laboratory and field observations of bacteria, microbial-sized microsphere, and bromide transport through aquifer sediments. Water Resour. Res. 29 (8), 2713–2721. https://doi.org/10.1029/93WR00963.

He, K., Retterer, S.T., Srijanto, B.R., Conrad, J.C., Krishnamoorti, R., 2014. Transport and dispersion of nanoparticles in periodic nanopost arrays. ACS Nano 8 (5), 4221–4227. https://doi.org/10.1021/nn404497z.

Herrick, M.G., Benson, D.A., Meerschaert, M.M., McCall, K.R., 2002. Hydraulic conductivity, velocity, and the order of the fractional dispersion derivative in a highly heterogeneous system. Water Resour. Res. 38 (11). https://doi.org/10.1029/2001WR000914, 9–1.

Hoffmann, R., Dassargues, A., Goderniauxf, P., Hermans, T., 2019. Heterogeneity and prior uncertainty investigation using a joint heat and solute tracer experiment in alluvial sediments. Front. Earth Sci. 7, 108. https://doi.org/10.3389/feart.2019.00108.

Hong, Y., Honda, R.J., Myung, N.V., Walker, S.L., 2009. Transport of iron-based nanoparticles: role of magnetic properties. Environ. Sci. Technol. 43 (23), 8834–8839. https://doi.org/10.1021/es9015525.

Huysmans, M., Dassargues, A., 2005. Review of the use of Péclet numbers to determine the relative importance of advection and diffusion in low permeability environments. Hydrogeol. J. 13, 895–904. https://doi.org/10.1007/s10040-004-0387-4.

Illman, W.A., Berg, S.J., Yeh, T.C.J., 2012. Comparison of approaches for predicting solute transport: sandbox experiments. Groundwater 50 (3), 421–431. https://doi.org/10.1111/j.1745-6584.2011.00859.x.

Johnson, W.P., Pazmino, E., Ma, H., 2010. Direct observations of colloid retention in granular media in the presence of energy barriers, and implications for inferred mechanisms from indirect observations. Water Res. 44 (4), 1158–1169. https://doi.org/10.1016/j.watres.2009.12.014.

Jose, S.C., Rahman, M.A., Cirpka, O.A., 2004. Large-scale sandbox experiment on longitudinal effective dispersion in heterogeneous porous media. Water Resour. Res. 40 (12). https://doi.org/10.1029/2004WR003363.

Keller, A.A., Sirivithayapakorn, S., Chrysikopoulos, C.V., 2004. Early breakthrough of colloids and bacteriophage MS2 in a water-saturated sand column. Water Resour. Res. 40 (8). https://doi.org/10.1029/2003WR002676.

Kianfar, B., Tian, J., Rozemeijer, J., van der Zaan, B., Bogaard, T.A., Foppen, J.W., 2022. Transport characteristics of DNA-tagged silica colloids as a colloidal tracer in saturated sand columns; role of solution chemistry, flow velocity, and sand grain size. J. Contam. Hydrol. 246, 103954. https://doi.org/10.1016/j.jconhyd.2022.103954.

Ko, C.H., Elimelech, M., 2000. The "shadow effect" in colloid transport and deposition dynamics in granular porous media: measurements and mechanisms. Environ. Sci. Technol. 34 (17), 3681–3689. https://doi.org/10.1021/es0009323.

Kong, X.Z., Deuber, C.A., Kittilä, A., Somogyvári, M., Mikutis, G., Bayer, P., Saar, M.O., 2018. Tomographic reservoir imaging with DNA-labeled silica nanotracers: the first field validation. Environ. Sci. Technol. 52 (23), 13681–13689. https://doi.org/10.1021/acs.est.8b04367.

Konikow, L.F., Hornberger, G.Z., Halford, K.J., Hanson, R.T., Harbaugh, A.W., 2009. Revised multi-node well (MNW2) package for MODFLOW ground-water flow model. US Geol. Surv. Techn. Methods 67 (10.3133). http://pubsdata.usgs.gov/pubs/tm/tm6a30/index.html.

Leij, F.J., Bradford, S.A., 2013. Colloid transport in dual-permeability media. J. Contam. Hydrol. 150, 65–76. https://doi.org/10.1016/j.jconhyd.2013.03.010.

Levy, M., Berkowitz, B., 2003. Measurement and analysis of non-Fickian dispersion in heterogeneous porous media. J. Contam. Hydrol. 64 (3–4), 203–226. https://doi.org/10.1016/S0169-7722(02)00204-8.

Li, J., Rajajayavel, S.R.C., Ghoshal, S., 2016. Transport of carboxymethyl cellulose-coated zerovalent iron nanoparticles in a sand tank: effects of sand grain size, nanoparticle concentration and injection velocity. Chemosphere 150, 8–16. https://doi.org/10.1016/j.chemosphere.2015.12.075.

Liang, X., Zhang, Y.K., 2013. Temporal and spatial variation and scaling of groundwater levels in a bounded unconfined aquifer. J. Hydrol. 479, 139–145. https://doi.org/10.1016/j.jhydrol.2012.11.044.

Liu, Q., Cui, X., Zhang, C., Huang, S., 2016. Experimental investigation of suspended particles transport through porous media: particle and grain size effect. Environ. Technol. 37 (7), 854–864. https://doi.org/10.1080/09593330.2015.1088578.

Liu, F., Yeh, T.C.J., Wang, Y.L., Hao, Y., Wen, J.C., Wang, W., 2020. Characterization of basin-scale aquifer heterogeneity using transient hydraulic tomography with aquifer responses induced by groundwater exploitation reduction. J. Hydrol. 588, 125137. https://doi.org/10.1016/j.jhydrol.2020.125137.

Lu, C., Yao, C., Su, X., Jiang, Y., Yuan, F., Wang, M., 2018. The influences of a clay lens on the hyporheic exchange in a sand dune. Water 10 (7), 826. https://doi.org/10.3390/w10070826.

Lyon-Marion, B.A., Becker, M.D., Kmetz, A.A., Foster, E., Johnston, K.P., Abriola, L.M., Pennell, K.D., 2017. Simulation of magnetite nanoparticle mobility in a heterogeneous flow cell. Environ. Sci. Nano 4 (7), 1512–1524. https://doi.org/10.1039/C7EN00152E.

Maier, R., Leven, C., Sánchez-León, E., Strasser, D., Stoll, M., Cirpka, O.A., 2022. Revealing vertical aquifer heterogeneity and hydraulic anisotropy by pumping partially penetrating wells. Hydrogeol. J. 30 (2), 463–477. https://doi.org/10.1007/s10040-022-02458-9.

Maxwell, R.M., Welty, C., Tompson, A.F., 2003. Streamline-based simulation of virus transport resulting from long term artificial recharge in a heterogeneous aquifer. Adv. Water Resour. 26 (10), 1075–1096. https://doi.org/10.1016/S0309-1708(03)00074-5.

Mikutis, G., Deuber, C.A., Schmid, L., Kittilä, A., Lobsiger, N., Puddu, M., Stark, W.J., 2018. Silica-encapsulated DNA-based tracers for aquifer characterization. Environ. Sci. Technol. 52 (21), 12142–12152. https://doi.org/10.1021/acs.est.8b03285.

Moeck, C., Radny, D., Popp, A., Brennwald, M., Stoll, S., Auckenthaler, A., Schirmer, M., 2017. Characterization of a managed aquifer recharge system using multiple tracers. Sci. Total Environ. 609, 701–714. https://doi.org/10.1016/j.scitotenv.2017.07.211.

Mohammaddost, A., Mohammadi, Z., Hussainzadeh, J., Farahmand, A., Sivelle, V., Labat, D., 2024. Evaluating Empirical, Field, and Laboratory Approaches for Estimating the Hydraulic Conductivity in the Kabul Aquifer. Water 16 (15), 2204.

Mohammadi, Z., Gharaat, M.J., Field, M., 2019. The effect of hydraulic gradient and pattern of conduit systems on tracing tests: bench-scale modeling. Groundwater 57 (1), 110–125. https://doi.org/10.1111/gwat.12659.

Mohammadi, Z., Illman, W.A., Field, M., 2021. Review of laboratory scale models of karst aquifers: approaches, similitude, and requirements. Groundwater 59 (2), 163–174.

Mondal, P.K., Furbacher, P.D., Cui, Z., Krol, M.M., Sleep, B.E., 2018. Transport of polymer stabilized nano-scale zero-valent iron in porous media. J. Contam. Hydrol. 212, 65–77. https://doi.org/10.1016/j.jconhyd.2017.11.004.

Morley, L.M., Hornberger, G.M., Mills, A.L., Herman, J.S., 1998. Effects of transverse mixing on transport of bacteria through heterogeneous porous media. Water Resour. Res. 34 (8), 1901–1908. https://doi.org/10.1029/98WR01210.

Müller, K., Vanderborght, J., Englert, A., Kemna, A., Huisman, J.A., Rings, J., Vereecken, H., 2010. Imaging and characterization of solute transport during two tracer tests in a shallow aquifer using electrical resistivity tomography and multilevel groundwater samplers. Water Resour. Res. 46 (3). https://doi.org/10.1029/2008WR007595.

Neshat, A., Pradhan, B., Javadi, S., 2015. Risk assessment of groundwater pollution using Monte Carlo approach in an agricultural region: an example from Kerman Plain, Iran. Comput. Environ. Urban. Syst. 50, 66–73. https://doi.org/10.1016/j.compenvurbsys.2014.11.004.

Oudega, T.J., Lindner, G., Derx, J., Farnleitner, A.H., Sommer, R., Blaschke, A.P., Stevenson, M.E., 2021. Upscaling transport of *Bacillus subtilis* endospores and coliphage phiX174 in heterogeneous porous media from the column to the field scale. Environ. Sci. Technol. 55 (16), 11060–11069. https://doi.org/10.1021/acs.est.1c01892.

Pang, L., Abeysekera, G., Hanning, K., Premaratne, A., Robson, B., Abraham, P., Billington, C., 2020. Water tracking in surface water, groundwater and soils using free and alginate-chitosan encapsulated synthetic DNA tracers. Water Res. 184, 116192. https://doi.org/10.1016/j.watres.2020.116192.

Phenrat, T., Cihan, A., Kim, H.J., Mital, M., Illangasekare, T., Lowry, G.V., 2010. Transport and deposition of polymer-modified Fe0 nanoparticles in 2-D heterogeneous porous media: effects of particle concentration, Fe0 content, and coatings. Environ. Sci. Technol. 44 (23), 9086–9093. https://doi.org/10.1021/es102398e.

Pool, M., Carrera, J., Alcolea, A., Bocanegra, E.M., 2015. A comparison of deterministic and stochastic approaches for regional scale inverse modeling on the Mar del Plata aquifer. J. Hydrol. 531, 214–229. https://doi.org/10.1016/j.jhydrol.2015.09.064.

Ptak, T., Piepenbrink, M., Martac, E., 2004. Tracer tests for the investigation of heterogeneous porous media and stochastic modelling of flow and transport—a review of some recent developments. J. Hydrol. 294 (1–3), 122–163. https://doi.org/10.1016/j.jhydrol.2004.01.020.

Qin, X., Hua, Y., Sun, H., Xie, J., Zhao, Y., 2020. Visualization study on aniline-degrading bacteria AN-1 transport in the aquifer with the low-permeability lens. Water Res. 186, 116329. https://doi.org/10.1016/j.watres.2020.116329.

Ren, X.W., Santamarina, J.C., 2018. The hydraulic conductivity of sediments: a pore size perspective. Eng. Geol. 233, 48–54. https://doi.org/10.1016/j.enggeo.2017.11.022.

Renard, P., Alcolea, A., Ginsbourger, D., 2013. Stochastic versus deterministic approaches. In: Environmental Modelling: Finding Simplicity in Complexity, pp. 133–149. https://doi.org/10.1002/9781118351475.ch8.

Rojas, R., Feyen, L., Dassargues, A., 2008. Conceptual model uncertainty in groundwater modeling: combining generalized likelihood uncertainty estimation and Bayesian model averaging. Water Resour. Res. 44 (12). https://doi.org/10.1029/2008WR006908.

Ronayne, M.J., Gorelick, S.M., Zheng, C., 2010. Geological modeling of submeter scale heterogeneity and its influence on tracer transport in a fluvial aquifer. Water Resour. Res. 46 (10). https://doi.org/10.1029/2010WR009348.

Roychowdhury, A., Pati, S.P., Kumar, S., Das, D., 2014. Effects of magnetite nanoparticles on optical properties of zinc sulfide in fluorescent-magnetic Fe3O4/ZnS nanocomposites. Powder Technol. 254, 583–590. https://doi.org/10.1016/j.powtec.2014.01.076.

Salamon, P., Fernàndez-Garcia, D., Gómez-Hernández, J.J., 2007. Modeling tracer transport at the MADE site: the importance of heterogeneity. Water Resour. Res. 43 (8). https://doi.org/10.1029/2006WR005522.

Sarris, T.S., Close, M., Abraham, P., 2018. Using solute and heat tracers for aquifer characterization in a strongly heterogeneous alluvial aquifer. J. Hydrol. 558, 55–71. https://doi.org/10.1016/j.jhydrol.2018.01.032.

Sharma, A.N., Luo, D., Walter, M.T., 2012. Hydrological tracers using nanobiotechnology: proof of concept. Environ. Sci. Technol. 46 (16), 8928–8936. https://doi.org/10.1021/es301561q.

Sharma, A., Foppen, J.W., Banerjee, A., Sawssen, S., Bachhar, N., Peddis, D., Bandyopadhyay, S., 2021. Magnetic nanoparticles to unique DNA tracers: effect of functionalization on Physico-chemical properties. Nanoscale Res. Lett. 16, 1–16. https://doi.org/10.1186/s11671-021-03483-5.

Sirivithayapakorn, S., Keller, A., 2003. Transport of colloids in saturated porous media: a pore-scale observation of the size exclusion effect and colloid acceleration. Water Resour. Res. 39 (4). https://doi.org/10.1029/2002WR001583.

Solovitch, N., Labille, J., Rose, J., Chaurand, P., Borschneck, D., Wiesner, M.R., Bottero, J.Y., 2010. Concurrent aggregation and deposition of TiO2 nanoparticles in a sandy porous media. Environ. Sci. Technol. 44 (13), 4897–4902. https://doi.org/10.1021/es1000819.

Song, Y., Hu, R., Liu, Q., Qiu, H., Hou, X., Qi, J., Konadu-Amoah, B., 2023. Comparison of hydraulic travel time and attenuation inversions, thermal tracer tomography and geostatistical inversion for aquifer characterization: a numerical study. Water 15 (13), 2401. https://doi.org/10.3390/w15132401.

Sosa, J.I.M., Gutiérrez Anguamea, G.A., Monreal, R., Grijalva Noriega, F.J., Tapia-Villaseñor, E.M., 2022. Hydrogeomorphologic mapping of the transboundary San Pedro Aquifer: a tool for groundwater characterization. Water 14 (6), 906. https://doi.org/10.3390/w14060906.

Sun, N., Elimelech, M., Sun, N.Z., Ryan, J.N., 2001. A novel two-dimensional model for colloid transport in physically and geochemically heterogeneous porous media. J. Contam. Hydrol. 49 (3–4), 173–199. https://doi.org/10.1016/S0169-7722(00)00193-5.

Syngouna, V.I., Chrysikopoulos, C.V., 2011. Transport of biocolloids in water saturated columns packed with sand: effect of grain size and pore water velocity. J. Contam. Hydrol. 126 (3–4), 301–314. https://doi.org/10.1016/j.jconhyd.2011.09.007.

Tatti, F., Papini, M.P., Raboni, M., Viotti, P., 2016. Image analysis procedure for studying Back-Diffusion phenomena from low-permeability layers in laboratory tests. Sci. Rep. 6 (1), 30400. https://doi.org/10.1038/srep30400.

Tian, Y., Gao, B., Silvera-Batista, C., Ziegler, K.J., 2010. Transport of engineered nanoparticles in saturated porous media. J. Nanopart. Res. 12, 2371–2380. https://doi.org/10.1007/s11051-010-9912-7.

Torkzaban, S., Hocking, M., Bradford, S.A., Tazehkand, S.S., Sasidharan, S., Šimůnek, J., 2019. Modeling virus transport and removal during storage and recovery in heterogeneous aquifers. J. Hydrol. 578, 124082. https://doi.org/10.1016/j.jhydrol.2019.124082.

Tosco, T., Tiraferri, A., Sethi, R., 2009. Ionic strength dependent transport of microparticles in saturated porous media: modeling mobilization and immobilization phenomena under transient chemical conditions. Environ. Sci. Technol. 43 (12), 4425–4431. https://doi.org/10.1021/es900245d.

Tufenkji, N., Elimelech, M., 2004. Correlation equation for predicting single-collector efficiency in physicochemical filtration in saturated porous media. Environ. Sci. Technol. 38 (2), 529–536. https://doi.org/10.1021/es034049r.

Urumović, K., Urumović Sr., K., 2014. The effective porosity and grain size relations in permeability functions. Hydrol. Earth Syst. Sci. Discuss. 11 (6), 6675–6714. https://doi.org/10.5194/hessd-11-6675-2014.

Varouchakis, E.A., Hristopulos, D.T., 2013. Comparison of stochastic and deterministic methods for mapping groundwater level spatial variability in sparsely monitored basins. Environ. Monit. Assess. 185, 1–19. https://doi.org/10.1007/s10661-012-2527-y.

Vereecken, H., Döring, U., Hardelauf, H., Jaekel, U., Hashagen, U., Neuendorf, O., Seidemann, R., 2000. Analysis of solute transport in a heterogeneous aquifer: the Krauthausen field experiment. J. Contam. Hydrol. 45 (3–4), 329–358. https://doi.org/10.1016/S0169-7722(00)00107-8.

Vincent Henri, C., Harter, T., 2019. Stochastic assessment of nonpoint source contamination: joint impact of aquifer heterogeneity and well characteristics on management metrics. Water Resour. Res. 55 (8), 6773–6794. https://doi.org/10.1029/2018WR024230.

Wang, Y., Bradford, S.A., Šimůnek, J., 2013. Transport and fate of microorganisms in soils with preferential flow under different solution chemistry conditions. Water Resour. Res. 49 (5), 2424–2436. https://doi.org/10.1002/wrcr.20174.

Ward, A.S., Kelleher, C.A., Mason, S.J., Wagener, T., McIntyre, N., McGlynn, B., Payn, R. A., 2017. A software tool to assess uncertainty in transient-storage model parameters using Monte Carlo simulations. Freshw. Sci. 36 (1), 195–217. https://doi.org/10.1086/690444.

Won, J., Burns, S.E., 2017. Influence of ionic strength on clay particle deposition and hydraulic conductivity of a sand medium. J. Geotech. Geoenviron. Eng. 143 (10), 04017081. https://doi.org/10.1061/(ASCE)GT.1943-5606.0001780.

Won, J., Choo, H., Burns, S.E., 2020. Impact of solution chemistry on deposition and breakthrough behaviors of kaolinite in silica sand. J. Geotech. Geoenviron. Eng. 146 (1), 04019123. https://doi.org/10.1061/(ASCE)GT.1943-5606.0002199.

Yin, M., Ma, R., Zhang, Y., Chen, K., Guo, Z., Zheng, C., 2022. A dual heterogeneous domain model for upscaling anomalous transport with multi-peaks in heterogeneous aquifers. Water Resour. Res. 58 (4). https://doi.org/10.1029/2021WR031128 e2021WR031128.

Zha, Y., Yeh, T.C.J., Illman, W.A., Mok, C.M.W., Tso, C.H.M., Carrera, B.A., Wang, Y.L., 2019. Exploitation of pump-and-treat remediation systems for characterization of hydraulic heterogeneity. J. Hydrol. 573, 324–340. https://doi.org/10.1016/j.jhydrol.2019.03.089.

Zhang, Q., Raoof, A., Hassanizadeh, S.M., 2015. Pore-scale study of flow rate on colloid attachment and remobilization in a saturated micromodel. J. Environ. Qual. 44 (5), 1376–1383. https://doi.org/10.2134/jeq2015.01.0058.

Zhang, Y., Hartung, M.B., Hawkins, A.J., Dekas, A.E., Li, K., Horne, R.N., 2021. DNA tracer transport through porous media—the effect of DNA length and adsorption. Water Resour. Res. 57 (2). https://doi.org/10.1029/2020WR028382, 2020WR028382.

Zheng, C., Wang, P.P., 1999. MT3DMS: A Modular Three-Dimensional Multispecies Transport Model for Simulation of Advection, Dispersion, and Chemical Reactions of Contaminants in Groundwater Systems; Documentation and User's Guide. http://hdl.handle.net/11681/4734.